International Journal of Nanomedicine

Dovepress
open access to scientific and medical research

Open Access Full Text Article

ORIGINAL RESEARCH

Bacteria-Driven Tumor Microenvironment-Sensitive Nanoparticles Targeting Hypoxic Regions Enhances the Chemotherapy Outcome of Lung Cancer

Huan Shi[1,*], Lan Chen[2,*], Yanlin Liu[1,*], Qinglian Wen[1], Sheng Lin[1], Qian Wen[1], Yun Lu[1], Jie Dai[1], Jianmei Li[1], Susu Xiao[1], Shaozhi Fu[1]

[1]Department of Oncology, the Affiliated Hospital of Southwest Medical University, Luzhou, People's Republic of China; [2]Department of Oncology, the Affiliated Traditional Chinese Medicine Hospital of Southwest Medical University, Luzhou, People's Republic of China

*These authors contributed equally to this work

Correspondence: Shaozhi Fu, Tel +86 830-3165698, Fax +86 830-3165690, Email shaozhifu513@163.com

Background: Chemotherapy still plays a dominant role in cancer treatment. However, the inability of conventional chemotherapeutic drugs to reach the hypoxic zone of solid tumors significantly weakens their efficacy. Bacteria-mediated drug delivery systems can be an effective targeting strategy for improving the therapeutic outcomes in cancer. Anaerobic bacteria have the unique ability to selectively transport drug loads to the hypoxic regions of tumors.

Methods: We designed a *Bifidobacterium infantis* (Bif)-based biohybrid (Bif@PDA-PTX-NPs) to deliver polydopamine (PDA)-coated paclitaxel nanoparticles (PTX-NPs) to tumor tissues.

Results: The self-driven Bif@PDA-PTX-NPs maintained the toxicity of PTX as well as the hypoxic homing tendency of Bif. Furthermore, Bif@PDA-PTX-NPs significantly inhibited the growth of A549 xenografts in nude mice, and prolonged the survival of the tumor-bearing mice compared to the other PTX formulations without any systemic or localized toxicity.

Conclusion: The Bif@PDA-PTX-NPs biohybrids provide a new therapeutic strategy for targeted chemotherapy to solid tumors.

Keywords: tumor hypoxia, bifidobacterium infantis, paclitaxel, nanoparticles, lung cancer

Introduction

Hypoxia is a prevalent characteristic of most solid tumors and limits the efficacy of chemotherapy.[1,2] Most conventional therapeutic drugs cannot penetrate into the deeper hypoxic regions of tumor tissues.[3] This not only lowers the intratumoral drug concentration but also results in off-target effects,[4] eventually leading to treatment failure due to systemic toxicity. Therefore, the current focus of cancer therapies is to specifically deliver chemotherapeutic drugs to the hypoxic regions of tumors[5,6] using nanoparticle (NP) carriers, biological camouflage[7,8] or magnetic induction[9] in order to increase the effective drug concentration in tumor tissues. NPs are preferable drug carriers since they can improve the water solubility of hydrophobic drugs, release drugs continuously and prolong their circulation in blood.[10,11] The diblock copolymer methoxy poly(ethylene glycol)-poly(ε-caprolactone) (mPEG-PCL) consists of hydrophobic PCL segments and hydrophilic mPEG segments that self-assemble into micelles in water, which can be used to load hydrophobic antineoplastic drugs. Chemotherapeutic drugs can be delivered to the tumor site using mPEG-PCL NP carriers.[12–14] However, NPs usually enter tumor tissue passively by means of the enhanced permeability and retention (EPR) effect, wherein they pass through blood circulation to reach the microvessels in the tumor.[1] Although the EPR-dependent nanoformulations have achieved good therapeutic effects in tumor-bearing mouse models, the EPR effect has not been observed in the human body, which obfuscates the clinical potential of these NPs.[15] Actively targeting NPs have been designed by grafting biorecognition molecules (ligands) onto their surface. Although these NPs can directly deliver anticancer drugs to tumor tissues via ligand-receptor binding and increase drug uptake by tumor cells,[16] their accessibility to

Received: 9 November 2022
Accepted: 29 January 2023
Published: 15 March 2023

the hypoxic areas of solid tumors is still limited.[17,18] Therefore, it is necessary to construct new drug delivery systems for targeting the hypoxic tumor tissues.

Bacteria have long been used to treat human diseases,[19] and anaerobic bacteria that can effectively aggregate in hypoxic regions of tumors can be used as natural drug carriers for targeted therapy.[20] Studies show that photosynthetic bacteria,[5] Salmonella[21] and E. coli[22] can actively target to the hypoxic areas of malignant tumors after intravenous injection. Biohybrids of anaerobic bacteria and multifunctional NPs can selectively deliver chemotherapeutic drugs, photothermal agents or immunotherapeutic drugs to the hypoxic regions of solid tumors. However, most biohybrids reported so far use pathogenic bacteria rather than probiotics.[23,24] *Bifidobacterium infantis* (Bif) is a probiotic, anaerobic bacteria that is harmless to humans and does not require any genetic modification.[25,26] Bif can be combined with nano-drugs in vitro or through antigen-antibody binding in vivo to form biohybrids for targeted drug delivery to hypoxic tumor zones.[27,28]

Given the affinity of bacteria to proteins, we previously constructed a bacteria-driven biohybrid drug carrier by directly attaching drug-loaded albumin NPs to bacterial cells.[27] However, the NPs were easily dislodged from the bacterial cells due to the impact of blood flow, which reduced the efficiency of the biohybrids. To overcome this limitation, we coated the NPs with the biocompatible polydopamine (PDA), which can not only strengthen the adhesion of NPs to the bacterial cells but also prevent early drug release.[12,29] As shown in Scheme 1, we synthesized paclitaxel-loaded NPs (PTX-NPs) using mPEG-PCL copolymer as the carrier, and coated the surface with PDA. The PDA-PTX-NPs were incubated with Bif cells to generate the Bif@PDA-PTX-NPs hybrids. Once these biohybrids reach the hypoxic zone of tumor tissues, the PTX-NPs are released in response to the reductive tumor environment and taken up by the

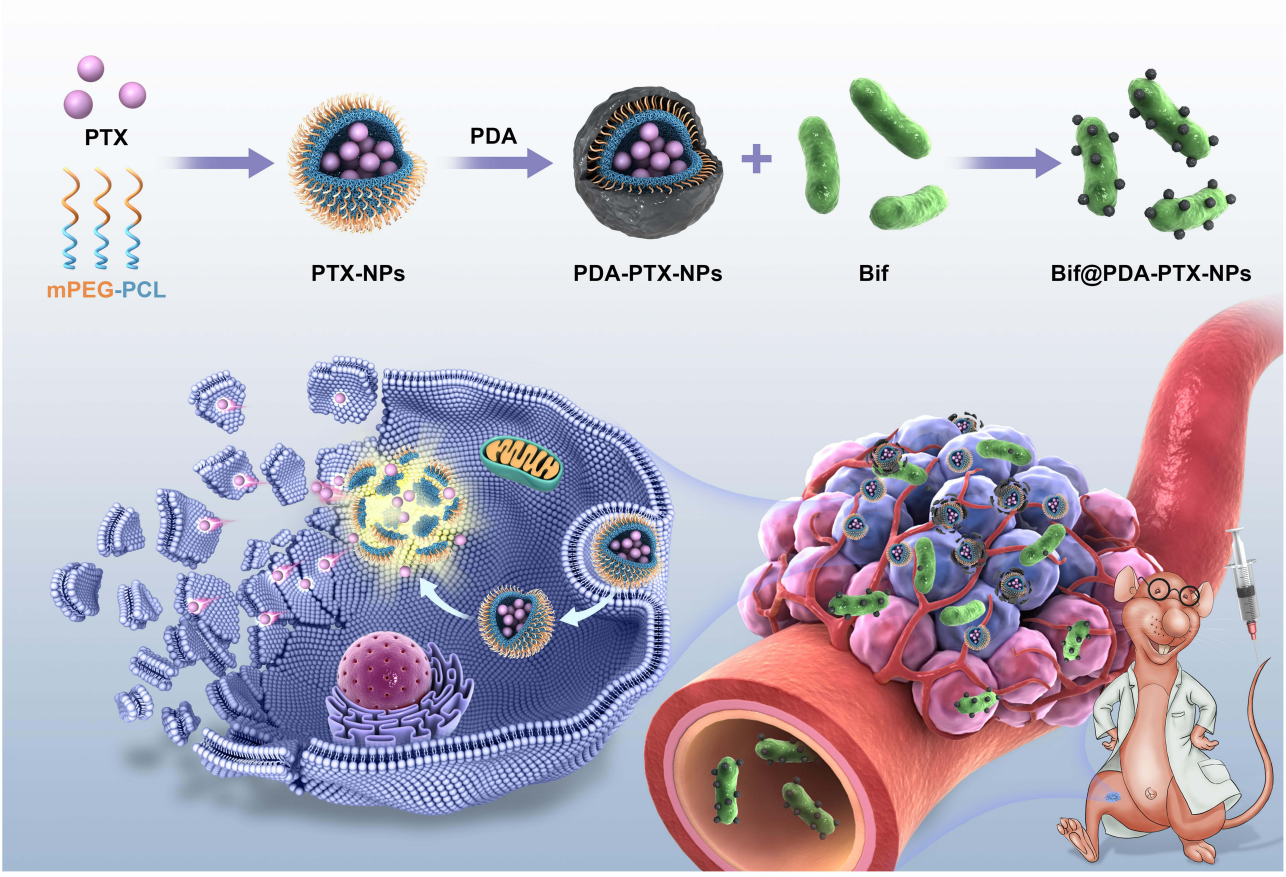

Scheme 1 Schematic diagram shows the construction of the Bif@PDA-PTX-NPs biohybrid and its intelligent responsibility to reductive tumor microenvironment through self-driven targeting to hypoxic regions of tumor.

tumor cells.[30–32] The anti-tumor effects of Bif@PDA-PTX-NPs were evaluated in vitro as well as a murine lung cancer model.

Materials and Methods

Materials

Monomethoxy PEG (mPEG, molecular weight Mn=2000 Da), ε-caprolactone (ε-CL) and dopamine hydrochloride were purchased from Macklin Biochemical Co. Ltd. (Shanghai, China). Stannous octoate ($Sn(Oct)_2$) was obtained from Sigma-Aldrich Trading Co. Ltd. (USA), and paclitaxel from Meilun Biological Technology Co. Ltd. (Dalian, China). *B. infantis* (GIMI.207) was provided by the Strains Preservation Center of Guangzhou Institute of Microbiology (Guangdong, China), and incubated anaerobically on agar plates at 37°C for 48 hours. A549 cells were purchased from the Cell Bank of Chinese Academy of Sciences (Shanghai, China). Male nude mice weighting 16–18 g (6 weeks of age) were supplied by Tengxin Biological Technology Co. Ltd. (Chongqing, China). All animal experimental procedures were approved by the Ethics and Science Committee of the Animal Care and Treatment Committee of Southwest Medical University and followed the Chinese National Guidelines (GB/T 35892-20181). The mice were housed in specific pathogen-free conditions at 24°C and relative humidity of 50–60% under a 12h-light/12h-dark schedule, with ad libitum access to standard rodent food and tap water. All mice were healthy and had no infection during the experimental period.

Preparation and Characterization of PTX-NPs, PDA-PTX-NPs and Bif@PDA-PTX-NPs

The diblock copolymer mPEG-PCL was synthesized from ε-CL and mPEG by ring-opening copolymerization with Sn $(Oct)_2$ as the catalyst. Briefly, equal amounts of mPEG and ε-CL were put in a glass bottle along with $Sn(Oct)_2$ (0.5% w/w of the total reactants), and the bottle was connected to a vacuum system. The mixture was heated at 130°C for 6 h, and the crude product was dissolved in dichloromethane and precipitated in ice-cooled petroleum ether. The purified mPEG-PCL copolymer was vacuum-dried and stored at 4°C for further use.

To prepare PTX-NPs, 10 mg PTX and 50 mg mPEG-PCL were dissolved in 4 mL anhydrous ethanol, and the solution was placed on a rotary evaporator and heated at 60°C to remove ethanol. Five milliliters of preheated deionized water at 60°C was then added, and the bottle was slightly oscillated to enable self-assembly into PTX-NPs. The morphology of PTX-NPs was observed by transmission electron microscopy (TEM, Tecnai G2 F30, FEI, USA). Particle size and zeta potential were measured using dynamic light scattering (DLS, NanoBrook90 plus Zeta, Brookhaven, NY) at 25°C. Drug loading (DL) and encapsulation efficiency (EE) were determined by HPLC (Agilent 1260, Agilent Technologies, USA) and calculated according to the following equations.

$$\mathrm{DL} = \frac{PTX}{PTX + mPEG - PCL} \times 100\%$$

$$\mathrm{EE} = \frac{Actual\ DL}{Theoretical\ DL} \times 100\%$$

PDA-PTX-NPs were produced by coating PTX-NPs with a PDA layer through dopamine. Briefly, 50 mg PTX-NPs and 20 mg dopamine were dissolved in 50 mL Tris-HCl buffer (10 mM, pH=8.5) and stirred in the dark for 6h. The product was then centrifuged at 15,000 rpm for 10 min, and washed twice to remove unreacted dopamine. The morphology of the PDA-PTX-NPs was observed by scanning electron microscopy (SEM, SU8020, Japan). Particle size and zeta potential were measured by DLS as described above. To construct Bif@PDA-PTX-NPs biohybrids, 1 mg/mL PDA-PTX-NPs were incubated with a suspension of Bif (2×10^7 CFU/mL) at 37°C for 3 h. The mixture was then centrifuged at 2400 rpm for 4 mins, following which the supernatant was discarded and the sediment was washed twice with PBS (pH=7.4) to obtain the Bif@PDA-PTX-NPs biohybrids. Nile red (NR)-labeled hybrids (Bif@PDA-NR-NPs) were prepared by the same method. The surface morphology of Bif@PDA-PTX-NPs was analyzed by SEM (SU8020, Japan). The UV absorption spectra of PDA, PDA-PTX-NPs, Bif and Bif@PDA-PTX-NPs were analyzed to verify the successful preparation of the biohybrid. To investigate the effect of different concentrations of Bif on PTX loading, biohybrids were prepared using PDA-PTX-NPs (1 mg/mL, 2 mL) and different bacterial loads (2×10^5CFU/mL, 2×10^6CFU/mL, 2×10^7CFU/mL,

2×10^8CFU/mL, and 2×10^9CFU/mL) as described. The different Bif@PDA-PTX-NPs were disintegrated using acetonitrile to release PTX, and the amount of the released drug was determined by HPLC. To determine the potential effect of PDA coating on bacterial growth, freshly prepared Bif@PDA-PTX-NPs and Bif were respectively inoculated into the culture medium and incubated for 48 h. The number of viable bacterial cells was counted as per standard methods.

In vitro Drug Release

In vitro drug release was measured using a dialysis method. Briefly, free PTX, PTX-NPs or PDA-PTX-NPs were dispersed in PBS (pH=7.4) and put into dialysis bags with molecular weight cutoff of 3500 Da. The dialysis bags were placed in 40 mL PBS (pH=7.4, 6.8, 5.5) containing Tween 80 (0.5%, w/w) in 50 mL centrifuge tubes, and shaken at 100 rpm at 37°C in the dark. At different time points (1, 3, 6, 12, 24, 48, 72, 96, 120, 144 and 168 h), 2 mL aliquots were taken and replaced with the same volume of fresh PBS. The amount of drug in the medium was measured by HPLC (Agilent 1260, Agilent Technologies, USA).

In vitro Functional Assays

For the cytotoxicity assay, A549 cells were seeded into 96-well plates and incubated with free PTX, PTX-NPs, PDA-PTX-NPs or Bif@PDA-PTX-NPs for 24 h. MTT solution (5 mg/mL, 20 μL) was added to each well and the cells were incubated for 2 h. After dissolving the water-insoluble formazan crystals with 150 μL dimethyl sulfoxide, the optical density of each well at 490 nm was measured using the FLUOstar Omega microplate reader. For wound healing assay, A549 cells were cultured till confluent and the monolayer was scratched using a sterile pipette tip. After washing off the dislodged cells, fresh DMEM containing Bif@PDA-NPs, PTX, PDA-PTX-NPs or Bif@PDA-PTX-NPs was added, and the cells were incubated for 12 and 24 h. The wound areas were photographed at 0, 12 and 24 h, and the migration rate was calculated.

In vitro Uptake of NPs

To assess cellular uptake of the NPs, A549 cells were seeded in 6-well plates at the density of 2×10^5 cells/mL and incubated with normal saline (NS), Nile Red (NR), NR-loaded NPs (NR-NPs) or PDA-NR-NPs for 3 h. The cells were then stained with DAPI for 5 mins, washed thrice with PBS, and imaged under a fluorescence microscope (OLYMPUS, IX73, Japan).

Apoptosis Assay

A549 cells were seeded into 6-well plates (5×10^4/well) and incubated with NS, PTX, PTX-NPs, PDA-PTX-NPs, Bif@PDA-PTX-NPs or Bif@PDA-PTX-NPs along with 10mM GSH. The cells were harvested 24 h later, resuspended in staining buffer containing Annexin V and PI, and incubated for 15 minutes in the dark. The percentage of apoptotic cells was detected by flow cytometry (BD FACSVerse, Piscataway, NJ).

Transwell Assay

The ability of Bif to target hypoxic regions was ascertained in vitro by the transwell assay. The upper chambers of the transwell inserts were inoculated with 200 μL Bif suspension (5×10^7 CFU/mL) and the bottom chambers were filled with 0.4 mL mixture of glucose (0.4 mg/mL), glucose oxidase (0.5 kU) and catalase (0.5 kU). The oxidation of glucose by glucose oxidase depleted oxygen and produced hydrogen peroxide, which was quenched by catalase, resulting in an artificial hypoxic environment in vitro. In the control group, normoxic conditions were maintained in the bottom chamber. After 2 h of incubation, the number of bacterial cells that migrated to the bottom chambers was counted.

Evaluation of in vivo Distribution of Bif@PDA-PTX-NPs

To track the distribution of the hybrid NPs in vivo, the tumor-bearing mice were injected intravenously with normal saline (NS), Bif or Bif@PDA-PTX-NPs through the tail vein. After 48 hours, the tumor tissues, heart, liver, spleen, lungs, kidneys were harvested, and homogenized in sterile 0.1% Triton X-100. The tissue homogenates were serially diluted and plated on solid LB agar, and the plates were incubated in a hypoxic environment at 37°C for 48 h. The

ensuing colonies were counted and photographed. Furthermore, tumor tissues were sectioned and stained with FITC-labeled anti-Bif antibody (FITC@Ab) and Cy3-labeled anaerobic induction factor (Cy3@HIF-1α), and then counter-stained with DAPI. The co-localization of the bacteria and the hypoxic region was observed under a fluorescence microscope.

Establishment of Tumor Model and Treatment Regimen

A lung cancer model was established by inoculating 1×10^6 A549 cells (10^7 cells/mL) into the right leg of nude mice. Once the tumors grew to approximately 50–80 mm^3, the mice were randomly divided into the following groups (n=10 per group): normal saline (NS), Bif@PDA-NPs, PTX, PDA-PTX-NPs and Bif@PDA-PTX-NPs. The respective drugs were injected intravenously every other day for a week. The body weight and tumor volume of the mice were recorded during the entire observation period. Two days after the last dose, the heart, liver, spleen, lung and kidney were harvested and processed for H&E staining. The tumor tissues were harvested and stained with H&E, TUNEL and Ki-67 as per standard protocols.

Micro-PET/CT Scans

The early treatment response of tumors to different drugs was evaluated by micro-PET/CT scans (Siemens, Germany). Briefly, the mice were fasted for 6 h and then injected with 200–250 μCi ^{18}F-FDG through the tail vein. Thirty minutes later, the mice were anesthetized via isoflurane inhalation, and whole-body PET/CT scans were performed in two-dimensional mode (10 min per location emission scan) using the parameters of 80 kV, 500 mA and 1.5 mm slice collimation. The PET/CT images were analyzed by two nuclear medicine physicians. The regions of interest (ROIs) on the tumor images were manually drawn, and the maximum normalized uptake value (SUVmax) and mean uptake value (SUVmean) were calculated using the hottest individual pixel within the tumor.

Hematological Analysis

To assess systemic toxicity of Bif@PDA-PTX-NPs, blood samples were collected from the suitably treated mice via the retroorbital route, and the red blood cells (RBC), white blood cells (WBC), platelets (PLT), alanine aminotransferase (ALT), aspartate aminotransferase (AST), creatinine (CREA) and glomerular filtration rate (GFR) were measured.

In vitro Hemolysis Analysis

One milliliter of RBC suspension (2%, v/v) was mixed with 1 mL mPEG-PCL NPs, PDA-NPs or Bif@PDA-NPs. Double-distilled water and normal saline were respectively used as positive control and negative control. All samples were incubated at 37°C for 4 h and then centrifuged at 3000 rpm for 5 min. The optical density (OD) of the supernatant was measured at 540 nm using a UV-Vis spectrophotometer (UV-5800PC, Shanghai Metash Instruments Co. Ltd., Shanghai, China). The hemolysis rate was calculated according to the following equation.

$$Hemolyis\ Rate\ (\%) = \frac{OD\ value\ of\ experimental\ group - OD\ value\ of\ saline\ group}{OD\ value\ of\ postive\ control\ group - OD\ value\ of\ saline\ group} \times 100\%$$

Statistical Analysis

Statistical analysis was performed using GraphPad Prism 6.07 (GraphPad Software, Inc, San Diego, CA, USA). *t*-tests was used to evaluate the differences among groups. Results were expressed as mean ± SD (n=3). P-value<0.05 was considered statistically significant.

Results

Preparation and Characterization of the Different Nano-Formulations

TEM and SEM images clearly showed that the PTX-NPs and PDA-PTX-NPs were spherical and of uniform size (Figure 1A and B). Due to the PDA coating, the average particle size of PDA-PTX-NPs was significantly larger than that of PTX-NPs (297.7 nm vs 33.59 nm). In addition, the presence of PDA also decreased the zeta potential from −0.94 mV

to −16.90 mV (Figure S1). SEM imaging of the Bif@PDA-PTX-NPs revealed that the PDA-PTX-NPs adhered closely to the surface of bacterial cells (Figure 1C). Furthermore, the average particle size of the biohybrids was larger than that of naked Bif (Figure S2). The successful binding between PDA-PTX-NPs and Bif was also confirmed by the color change in the bacterial suspension (Figure 1Da-c). In addition, examination of the NR-labelled Bif@PDA-NR-NPs by confocal imaging indicated that PDA-NR-NPs were attached to the surface of Bif (Figure S3). UV-vis spectroscopy of the PDA-PTX-NPs and Bif@PDA-PTX-NPs further revealed a unique absorption peak of PDA at 240 nm that was absent in the PTX-NPs and Bif suspensions (Figure 1E). When the bacterial load was 2×10^7CFU/mL, the binding rate of PDA-PTX-NPs on Bif cells was 81.54% and the amount of PTX in the biohybrids was 203.85 μg/mL. Further increase in bacterial load had no significant effect on PTX concentration or the binding rate of the NPs (Figure 1F and Figure S4). Moreover, no obvious toxicity was observed in mice after intravenous injection of Bif suspension (2×10^7, 2×10^8, 2×10^9 and 2×10^{10}CFU/mL) (Figures S5–S7). Therefore, 2×10^7CFU/mL Bif was selected for in vivo experiments.

Bif@PDA-PTX-NPs Inhibited Tumor Cells in vitro

As shown in Figure 2A, PTX was released from the PTX-NPs and PDA-PTX-NPs at a significantly slower rate compared to free PTX over a period of 7 days, which is indicative of the sustained-release effect of nano-formulations. The slow-

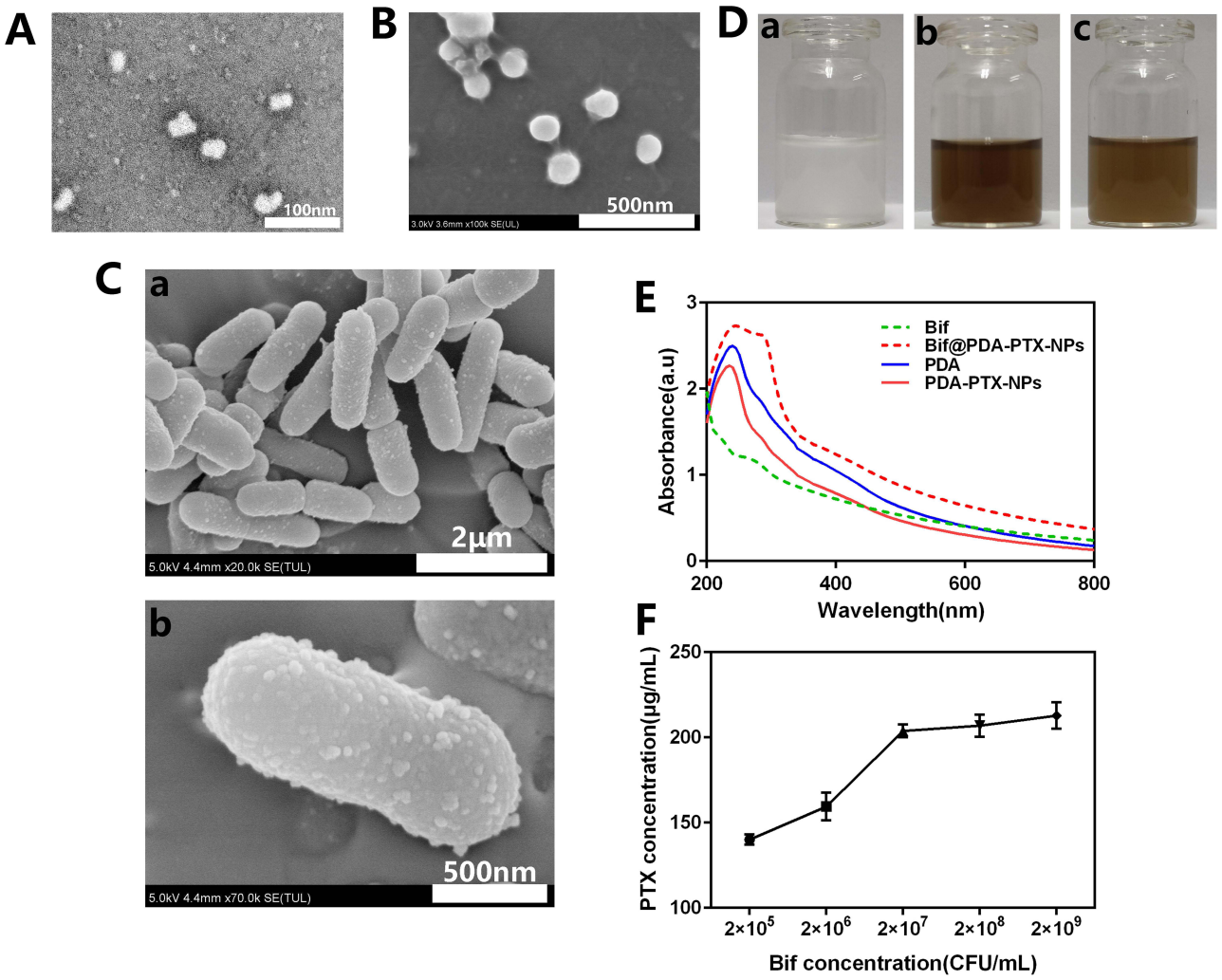

Figure 1 Characterization of PTX-NPs, PDA-PTX-NPs and Bif@PDA-PTX-NPs. (**A**) TEM image of PTX-NPs. (**B**) SEM image of PDA-PTX-NPs. (**C**) SEM images of Bif@PDA-PTX-NPs with different scale bars (a: 2 μm, b: 500 nm). (**D**) The photos indicate the color of Bif suspension, PDA-PTX-NPs and Bif@PDA-PTX-NPs in normal saline. [a]Bif; [b]PDA-PTX-NPs; [c]Bif@PDA-PTX-NPs. (**E**) UV-vis absorption curves of Bif, PDA, PDA-PTX-NPs and Bif@PDA-PTX-NPs. (**F**) the concentrations of PTX binding on the surface of Bif@PDA-PTX-NPs at different Bif concentrations (n=3, mean ± SD).

release pattern of PTX was similar at pH of 5.5 and 6.8 (Figure 2B and C). While mPEG-PCL did not show significant cytotoxicity compared to the blank NPs (Figure 2D), the PTX-NPs and PDA-PTX-NPs decreased the viability of A549 cells in a PTX concentration-dependent manner. The cytotoxic effect of free PTX was slightly greater than the NP-encapsulated drug (Figure 2E). Half-maximal inhibitory concentration (IC_{50}) values of each drug formulation were calculated as following: Free PTX (27.32±3.85μg/mL), PTX-NPs (40.08±1.78μg/mL), PDA-PTX-NPs (35.27±2.71μg/mL) and Bif@PDA-PTX-NPs (36.18±2.77μg/mL). As shown in Figure 2F and G, the wound healing rate in the control and Bif@PDA-NPs groups after 24h were 55.04% and 51.31% respectively, compared to only 9.4% in the Bif@PDA-PTX-NPs ($P<0.01$). Furthermore, the uptake of NR-NPs and PDA-NR-NPs by the A549 cells were higher compared to free NR, indicating that nano-scaled drug formulations can be more easily absorbed by tumor cells (Figure 3A and B).

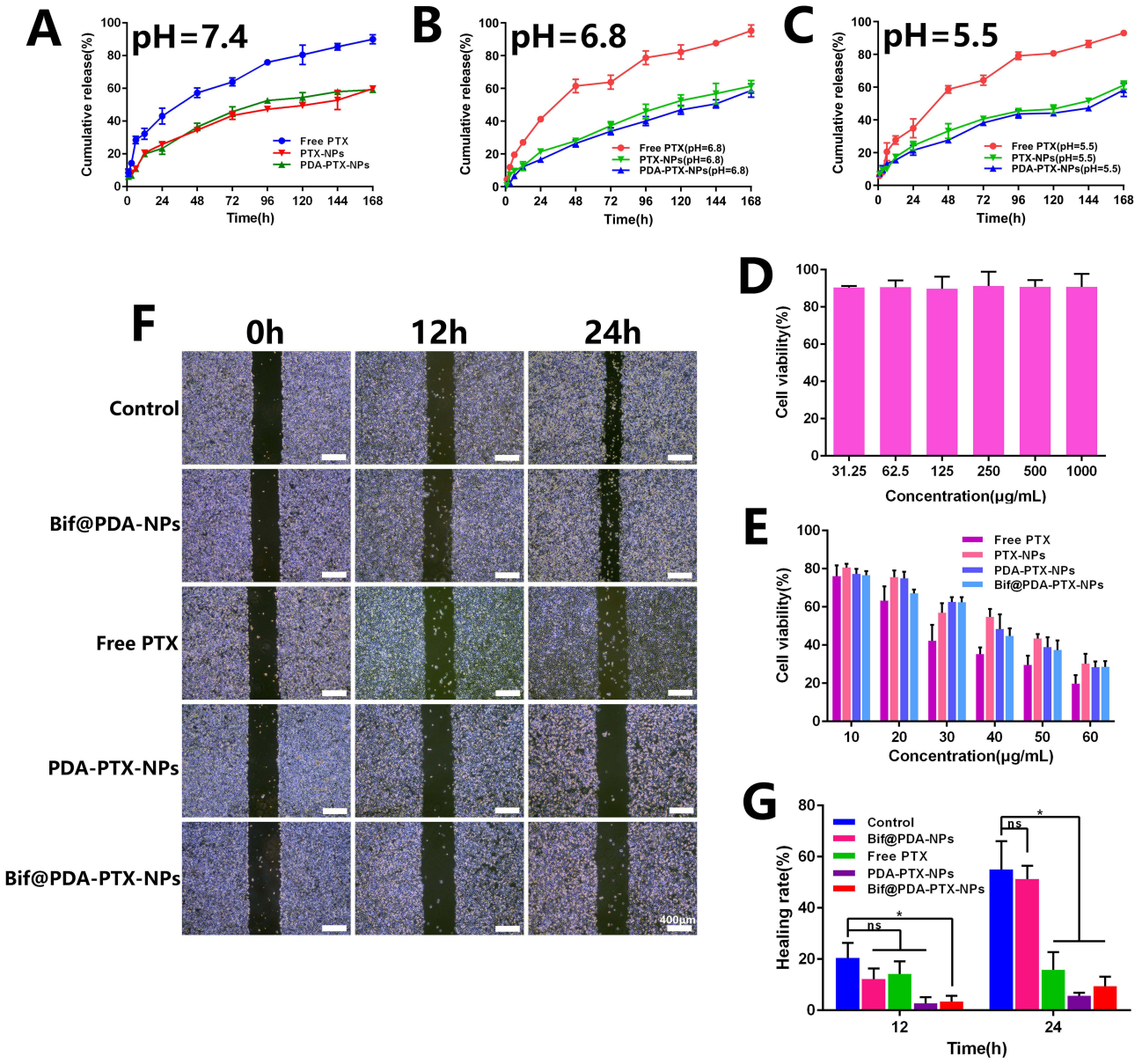

Figure 2 In vitro analysis of drug release profile and cytotoxicity. Drug release profile of Free PTX, PTX-NPs and PDA-PTX-NPs in PBS at pH 7.4 (**A**), pH 6.8(**B**) and pH 5.5 (**C**) (n=3, mean ± SD). (**D**) The cytotoxicity of mPEG-PCL nanoparticles on A549 cells (n=6). (**E**) The cytotoxicity of Free PTX, PTX-NPs, PDA-PTX-NPs and Bif@PDA-PTX-NPs on A549 cells. (**F**) Photos of wound healing (Scale bar=400 μm). (**G**) The healing rate of the groups of Control, Bif@PDA-NPs, Free PTX, PDA-PTX-NPs and Bif@PDA-PTX-NPs at 12 and 24 h. Data are presented as mean ± SD of three replicates (ns: no statistical significance, *P < 0.05).

The apoptosis rates of the cells treated with Bif@PDA-PTX-NPs and Bif@PDA-PTX-NPs + GSH were respectively 43.85% and 44.56%, and significantly higher than that in the untreated group (P<0.0001, Figure 3C and D).

Bif and Bif@PDA-PTX-NPs Selectively Accumulate in Hypoxic Regions

As shown in Figure 4A, the binding of PDA-PTX-NPs on the bacterial surface did not affect the biological activity of Bif. There was no significant difference in the number of colonies formed by the naked or NPs-bound bacteria (Figure S8). A hypoxic environment was simulated in vitro to assess the targeting ability of Bif (Figure 4B). As shown in Figure 4C, the bacterial counts in the hypoxic environment were significantly higher than that of the normoxic environment after 2 h of culture. Furthermore, tumor-bearing mice injected intravenously with Bif or Bif@PDA-PTX-NPs showed selective accumulation of Bif in the tumor tissues for 48 hours compared to the control group (Figure 4D), and only a miniscule amount of Bif was observed in the liver (Figure 4E). Consistent with this, the FITC-stained Bif (green) co-localized with the Cy3-stained hypoxic regions (red) of the tumor (Figure 4F–H), thus confirming bacterial accumulation in the tumor tissues. Taken together, Bif can selectively home to the hypoxic regions of solid tumor and colonize the tissues.

Bif@PDA-PTX-NPs Release the Loaded Drug Under Reductive Conditions

To evaluate the responsiveness of Bif@PDA-PTX-NPs to the reductive tumor microenvironment, we incubated the Nile Red (NR)-labelled biohybrids in PBS with or without GSH for 1 hour. As shown in Figure 5A, the GSH solutions underwent significant color change in the presence of Bif@PDA-PTX-NPs compared to the control. Furthermore, the color of the 10mM GSH solution was darker compared to that of 10μM GSH (Figure 5A). As shown in Figure 5B, UV absorbance curves also revealed a unique absorption peak at 550 nm corresponding to NR in 10 μM or 10 mM GSH but not in the control solution. Thus, a reductive tumor microenvironment containing high levels of GSH can disintegrate the PDA coating and dislodge PTX-NPs from the biohybrid. The dissociation rate of NR-NPs was significantly higher in response to 10 mM GSH compared to 10 μM GSH (Figure S9). As shown in Figure 5C and D, A549 cells incubated with the GSH supernatants absorbed the dissociated NPs, and the fluorescence intensity was higher with 10 mM compared to 10 μM GSH.

Bif@PDA-PTX-NPs Inhibited Tumor Growth in vivo

A549 tumor-bearing mice were used to evaluate in vivo anti-tumor effects of Bif@PDA-PTX-NPs, and the schematic diagram of the treatment regimen is shown in Figure 6A. Mice treated with Bif@PDA-PTX-NPs had the smallest tumors (Figure 6B and C), indicating the strongest inhibitory effect of the biohybrids on tumor growth compared to the other formulations. Consistent with this, the change in tumor volume was minimal in the Bif@PDA-PTX-NPs group (Figure 6D and E), which confirmed that the biohybrid significantly slowed tumor growth. In addition, there was no significant difference in the body weight among the treatment groups (Figure 6F). As shown in Figure 6G, the median survival durations of tumor-bearing mice in the NS, Bif@PDA-NPs, PTX and PTX-NPs groups were 50, 53, 57 and 69 days respectively, compared to 77 days in the Bif@PDA-PTX-NPs group. Moreover, micro-PET/CT images showed that ^{18}F-FDG uptake was weakest in the Bif@PDA-PTX-NPs group compared to the other groups (Figure 7A), and the respective SUV_{Max} values in the NS, Bif@PDA-NPs, PTX, PTX-NPs and Bif@PDA-PTX-NPs groups were 3.1±0.2, 3.133±0.153, 2.333±0.058, 0.727±0.031 and 0.643±0.015 respectively (Figure 7B). The SUV_{Mean} values also exhibited the same pattern, indicating that Bif@PDA-PTX-NPs significantly inhibited tumor metabolism. Ki-67 and TUNEL staining of the tumor tissues further showed that Bif@PDA-PTX-NPs decreased the proliferation rates of the tumor cells and increased apoptosis (Figure 7C and D). Finally, histopathological examination of tumor tissues revealed the Bif@PDA-PTX-NPs biohybrids decreased nuclear hyperchromasia in the tumor cells (Figure 7E). Taken together, the Bif@PDA-PTX-NPs biohybrids inhibited tumor growth and prolonged the survival of tumor-bearing mice.

Bif@PDA-PTX-NPs are Non-Hemolytic and Non-Toxic

To assess any possible hemolytic effects of the biohybrids, we incubated Bif@PDA-NPs with erythrocytes, and observed the hemolysis rates in terms of UV absorbance. As shown in Figure S10A–S10F, all erythrocytes in deionized water were ruptured, while those in the other groups (see methods) were almost non-ruptured. UV absorbance also indicated low

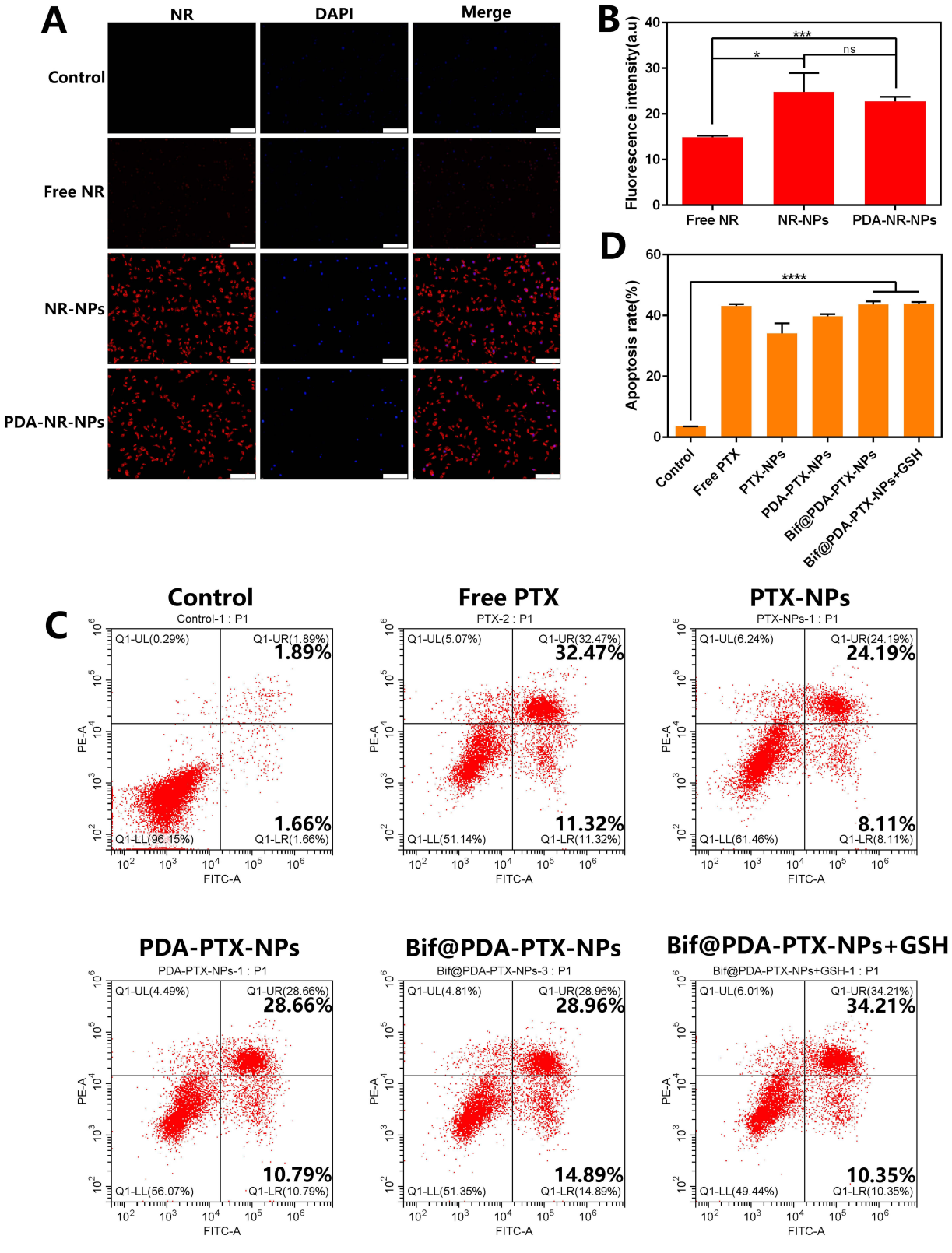

Figure 3 In vitro cellular uptake and flow cytometric analysis. (**A**) The cellular uptake of Control, Free NR, NR-NPs and PDA-NR-NPs groups (Scale bar=200μm). (**B**) The relative fluorescence intensity corresponding to cellular uptake. (n=3, ns: no statistical significance, *P < 0.05, ***P<0.001). (**C**) Cell apoptosis of A549 cells in the Control, Free PTX, PTX-NPs, PDA-PTX-NPs, Bif@PDA-PTX-NPs and Bif@PDA-PTX-NPs+GSH groups. (**D**) Quantitative results of apoptosis measured by flow cytometry. Data are presented as mean ± SD (n=3, ****P<0.0001).

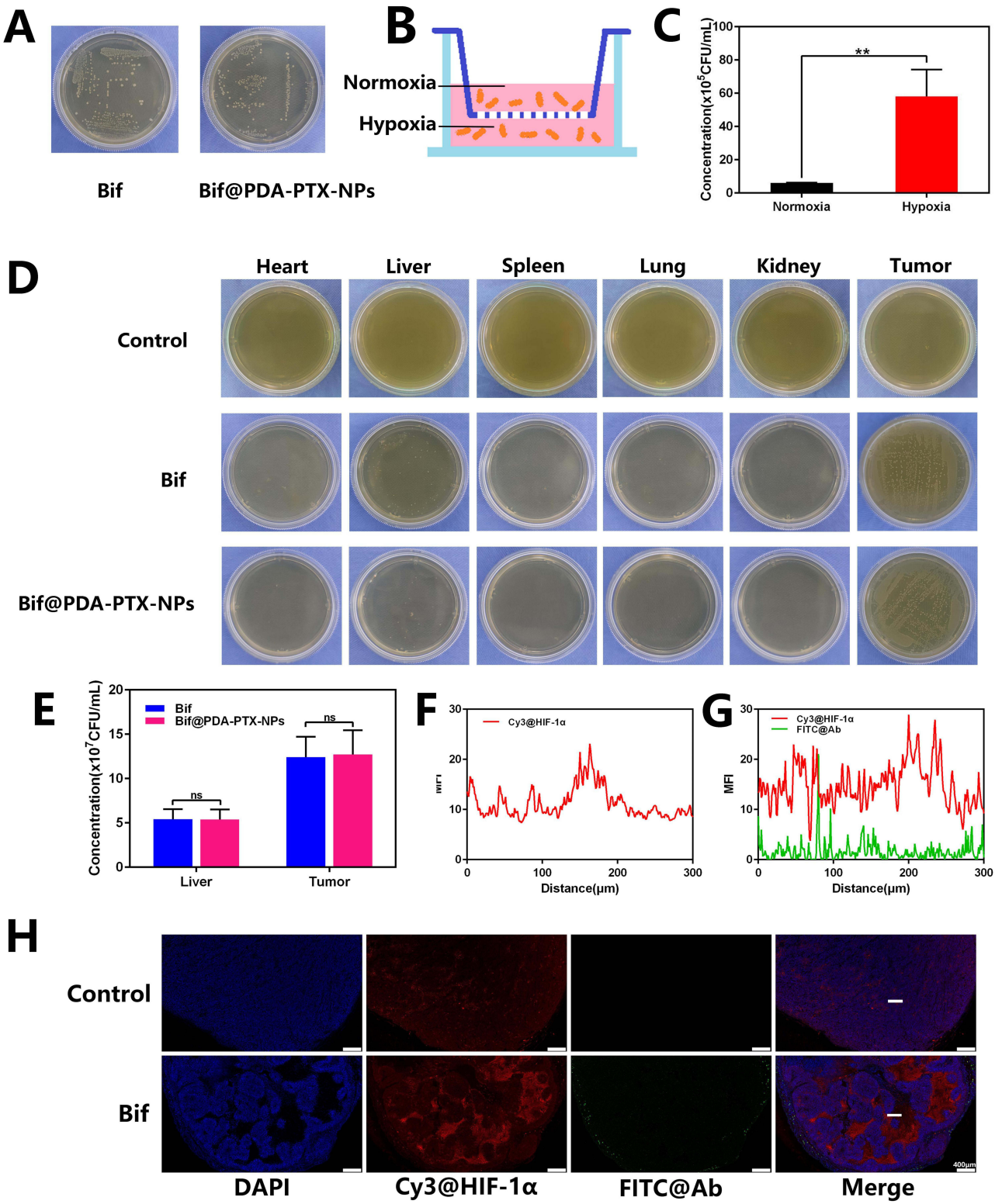

Figure 4 Evaluation of the targeting activity of the Bif@PDA-PTX-NPs biohybrid to hypoxic environment. (**A**) Anaerobic incubation of Bif and Bif@PDA-PTX-NPs for 24 h. (**B**) Schematic illustration of the hypoxia simulation model using a Transwell system to evaluate the hypoxic targeting activity of the biohybrid Bif@PDA-PTX-NPs. (**C**) The number of bacteria migrating to the bottom chamber (hypoxic environment) in a Transwell model. (**D**) Homogenates of the organs and tumor tissues were cultured on agar plates under a hypoxic environment at 37°C for 2 days. (**E**) The number of Bif in liver and tumor tissues of mice. (**F** and **G**) Bif@PDA-PTX-NPs and hypoxic zone co-localization in vivo. Hypoxic zone was stained in red with Cy3@HIF-1α (Anaerobic induction factors labelled with Cy3), and Bif was stained in green with FITC@Ab (Bifidobacterium infantis antibodies labelled with FITC). (**H**) Fluorescence co-localization images of Bif@PDA-PTX-NPs and hypoxic regions of tumor (Scale bar=400 μm). Data are presented as mean ± SD (n=3, ns: no statistical significance, **P<0.01).

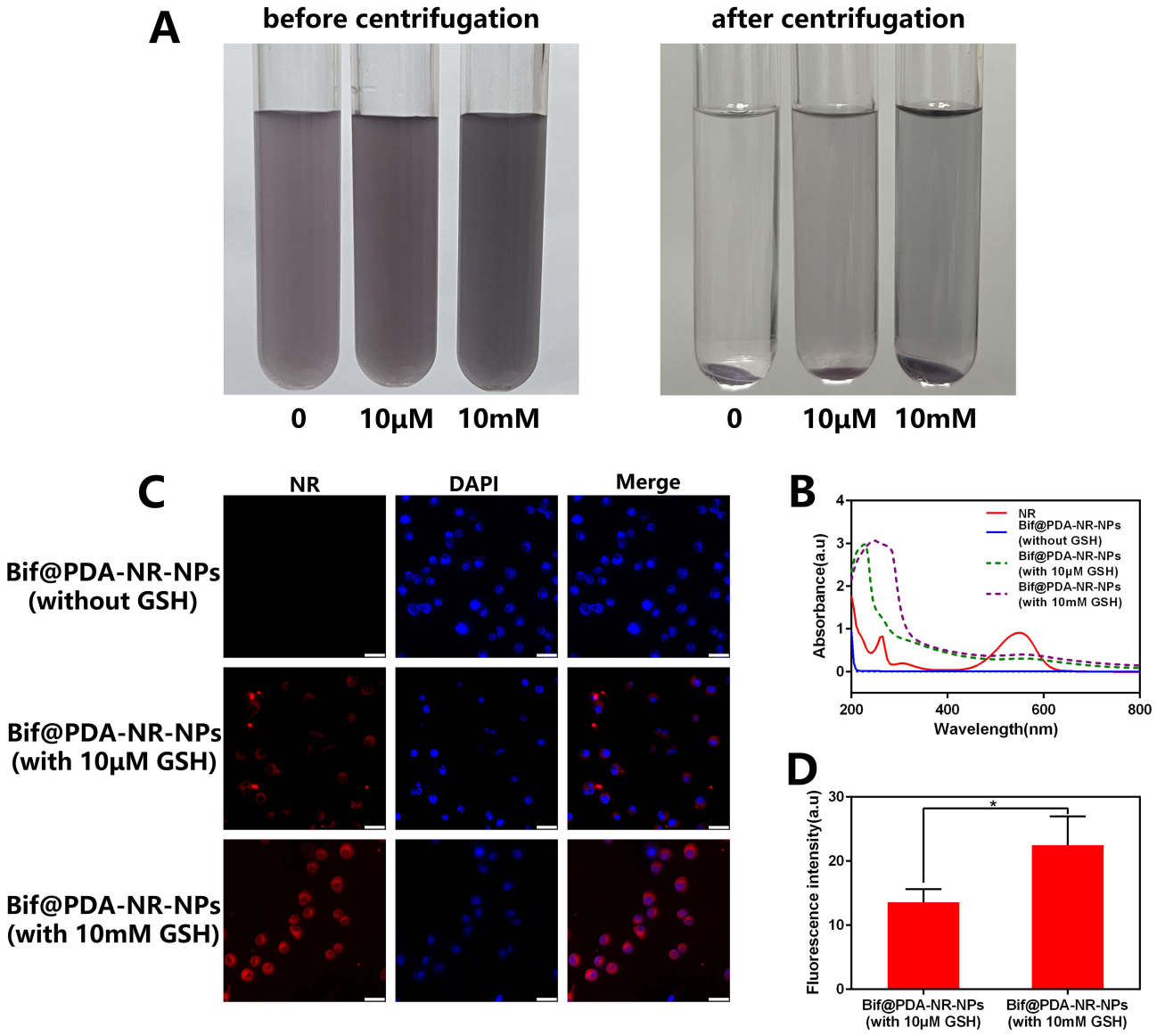

Figure 5 In vitro analysis of binding stability between Bif and PDA-NR-NPs. (**A**) After different concentrations of GSH were added to Bif@PDA-NR-NPs, the color of solutions changed before and after centrifugation. (**B**) UV-vis absorbance curves of supernatants after centrifugation. (**C**) The cellular uptake of supernatants in Bif@PDA-NR -NPs solutions with different GSH concentrations (Scale bar=40μm). (**D**) The relative fluorescence intensity corresponding to cellular uptake. Data are presented as mean ± SD (n=3, *P < 0.05).

hemolysis rate in the Bif@PDA-NPs group (Figure S10G and S10H), indicating good blood compatibility. Furthermore, H&E staining of vital organs, serum biochemical indices and blood count analysis of mice injected with the Bif@PDA-PTX-NPs did not indicate any obvious toxicity in the heart, liver, spleen, lung, kidney and blood system (Figure 8 and Figure S11). Thus, Bif@PDA-PTX-NPs are safe and can be administered intravenously.

Discussion

The rapid proliferation of tumor cells depletes oxygen and creates hypoxic conditions in solid tumors.[33] The tumor cells in these hypoxic regions are usually resistant to radiotherapy, chemotherapy, immunotherapy etc,[34] which can significantly affect therapeutic outcomes and patient prognosis.[35] Although numerous drug-loaded nano-formulations have been developed for anti-tumor therapy, their inability to accumulate in the hypoxic zones of solid tumors limits their applications.[36]

Anaerobic bacteria are promising carriers for the targeted delivery of therapeutic agents to hypoxic tumor tissues.[37] Chen et al used *Escherichia coli* to deliver NPs into tumors, and achieved rapid tumor cell death through magnetothermal

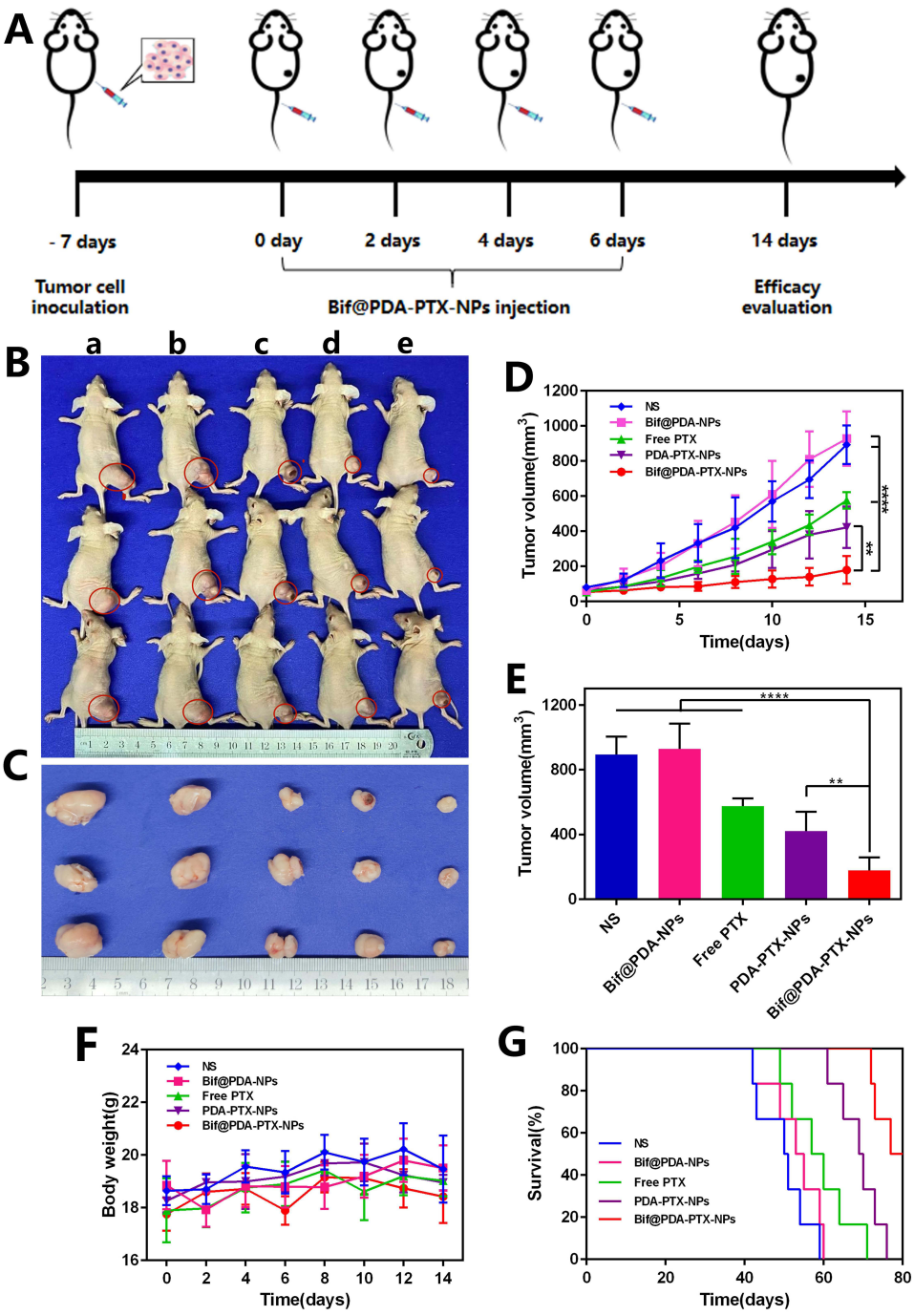

Figure 6 In vivo anti-tumor effect of Bif@PDA-PTX-NPs. (**A**) Schematic diagram of the treatment process. (**B**) The photos of tumor-bearing mice on the 14th day after different treatments. [a]Control, [b]Bif@PDA-NPs, [c]Free PTX, [d]PDA-PTX-NPs, [e]Bif@PDA-PTX-NPs. (**C**) The photos of isolated tumors. (**D**) The tumor volume growth curves of mice in different groups. (**E**) The tumor volume of mice in each group on day 14 of treatment (n=6, **P<0.01, ****P<0.0001). The body weight (**F**) and survival curves (**G**) of mice in each group. Data are presented as mean ± SD.

ablation and oxidative damage.[9] Furthermore, Yi et al successfully inhibited tumor growth in mice by simultaneously delivering photothermal and immunotherapeutic agents using *Salmonella*.[21] However, these bacteria are pathogenic and therefore need to be genetically modified or attenuated before use.[38,39] On the other hand, the obligate anaerobe *B. infantis* (Bif) is not only harmless to humans but can also target the hypoxic regions of solid tumors.[40–42] Intravenously administered Bif or its hybrid did not result in any significant toxicity in the heart, liver, spleen, lung, kidney and blood

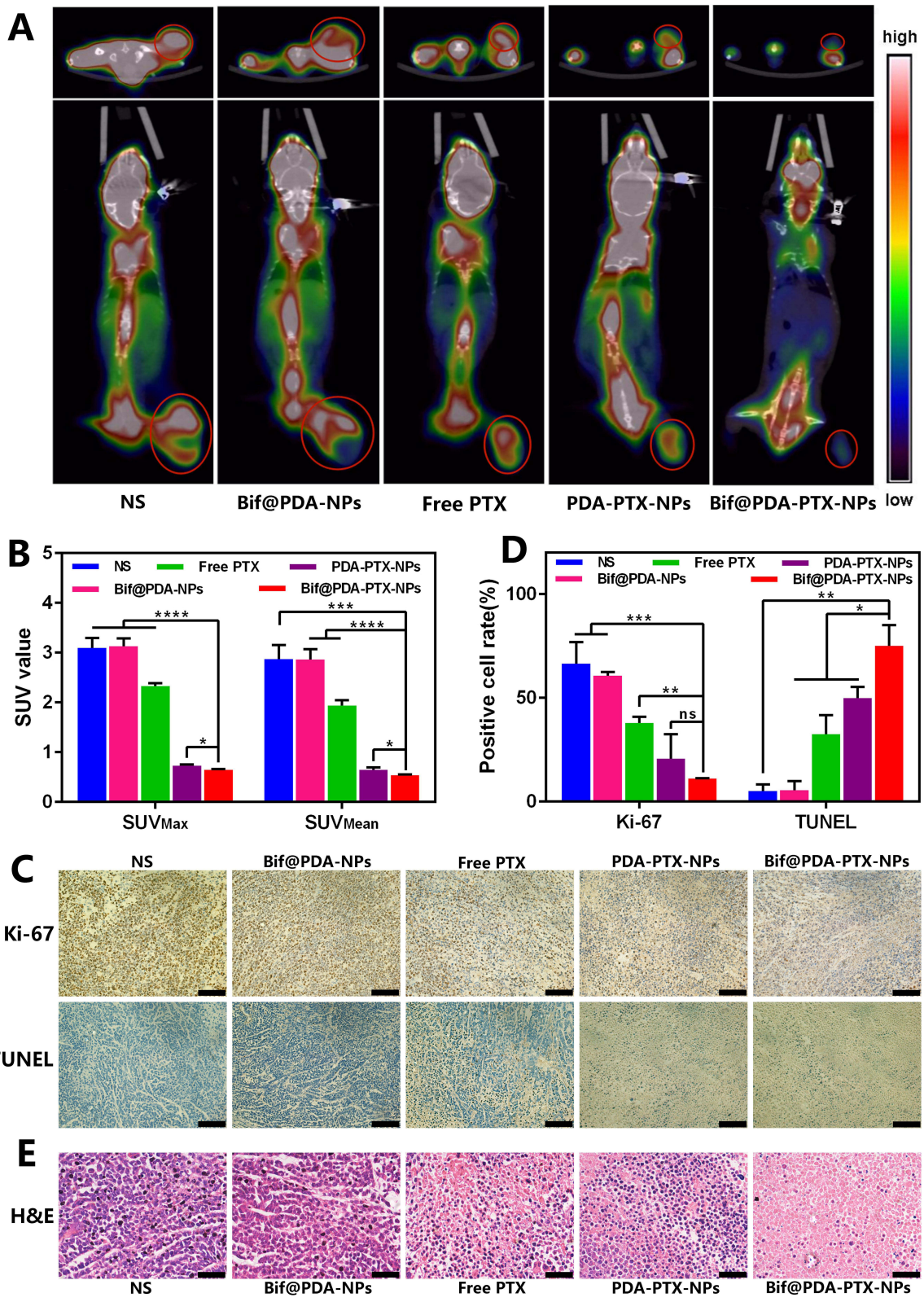

Figure 7 In vivo evaluation of anti-tumor efficacy on A549 tumor-bearing mice. (**A**) Representative ^{18}F-FDG PET/CT images of mice on day 14 of treatment, the upper layer shows the cross section of tumors, the lower layer displays the coronal images of mice. The red circles indicated the tumor sites. (**B**) SUVmax and SUVmean values of each group. (**C**) The immunohistochemical staining images of Ki-67 and TUNEL in tumor (Scale bar=100 μm). (**D**) The positive expression rates of Ki-67 and TUNEL staining. (**E**) The H&E staining images of tumor tissues (Scale bar=50 μm). Data are presented as mean ± SD (n=3, ns: no statistical significance, *P<0.05, **P<0.01, ***P<0.001, ****P<0.0001).

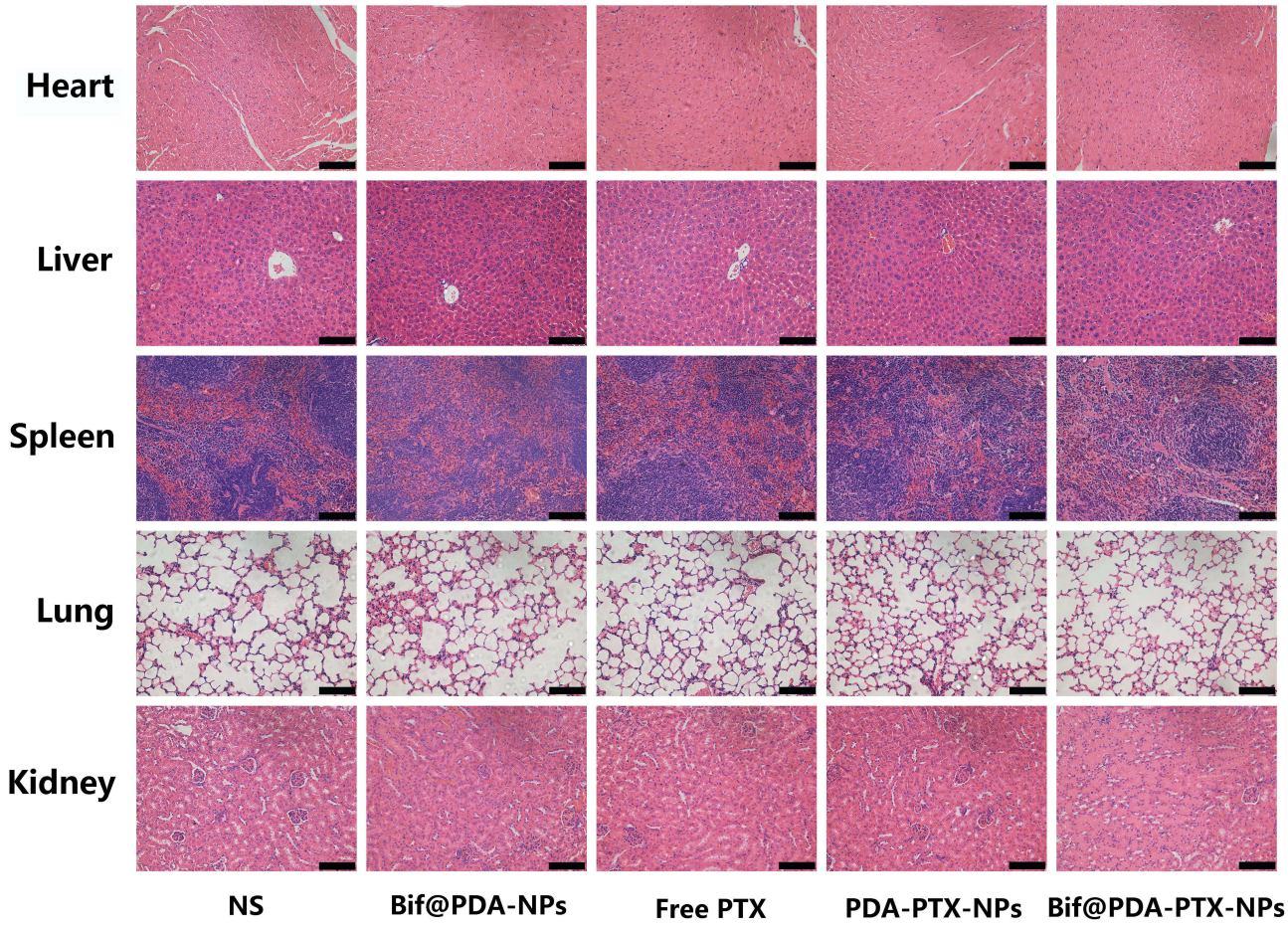

Figure 8 The H&E staining images of major organs (including heart, liver, spleen, lung and kidney) in each group after treatment. Scale bar=100 μm.

of mice.[27,28] Bif-mediated delivery of doxorubicin NPs to the hypoxic area of breast tumors improved the therapeutic outcome.[27] Therefore, Bif-based biohybrids are a safe and efficient drug delivery system for cancer treatment.

Bacterial cells and NPs can be conjugated through chemical bonds,[43] electrostatic adsorption,[44] antigen-antibody interactions[45] and so on. We used polydopamine (PDA) as the linker to connect PTX-NPs to Bif. PDA has the advantages of photothermal conversion, adhesion, excellent biocompatibility and non-toxicity.[46,47] The formation of a PDA shell through the self-polymerization of dopamine on the surface of NPs allows the latter to firmly adhere to the bacterial cells and prevents dislodgment in the bloodstream.[23] We confirmed that the PDA-mediated adhesion of PTX-NPs on the surface of Bif does not affect bacterial reproduction and migration.

Another advantage of the PDA linker is that it ensures targeted delivery of the biohybrid to the tumor tissue on account of its susceptibility to glutathione (GSH).[48] GSH is present at very low levels in normal tissues and blood circulation,[49] but increases to 10mM or even higher in the hypoxic tumors, which creates a highly reductive environment that can degrade PDA.[32] In our study, we verified that the Bif@PDA-NR-NPs biohybrid did not dissociate in a solution lacking GSH. In the presence of GSH however, the PDA coating was rapidly destroyed, which separated the NR-NPs from the Bif cells. These detached NPs were more easily absorbed by tumor cells. Therefore, the Bif@PDA-PTX-NPs biohybrid is a GSH-responsive drug delivery system that can selectively release the drugs in the reductive tumor microenvironment.

In this study, paclitaxel was encapsulated into the NPs using mPEG-PCL copolymer through a self-assembly method. The blank mPEG-PCL NPs were non-toxic even at the high concentration of 1000μg/mL, indicating their biosafety as a drug carrier for clinical applications. The biohybrid Bif@PDA-NPs also did not cause serious hemolysis, indicating that it can be administered via the intravenous route. Furthermore, sustained release of PTX-NPs from Bif@PDA-PTX-NPs

directly into the hypoxic zone of tumor tissues significantly inhibited the proliferation of tumor cells and promoted their apoptosis, without causing any significant toxicity in the vital organs.

To summarize, the Bif@PDA-PTX-NPs biohybrid can efficiently transport PTX to the hypoxic regions of solid tumors and improve the efficacy of chemotherapy. The surface modification with PDA not only improved the adherence of the NPs to the bacterial cells but may also exert a photothermal effect.[50–52] Therefore, the Bif@PDA-PTX-NPs biohybrid is a promising tool for combined chemotherapy and photothermal therapy against solid tumors.

Conclusion

We constructed Bif@PDA-PTX-NPs biohybrids by conjugating PTX-NPs with Bif cells using PDA as the linker. The biohybrid can actively accumulate in the hypoxic regions of solid tumors by virtue of the anaerobic bacteria. Furthermore, the high GSH concentration and acidic conditions in the tumor environment led to the detachment of the PTX-NPs from the bacterial cells, which then released the drugs in-situ in a sustained manner, thereby inhibiting tumor cell proliferation and enhancing apoptosis. Compared to other PTX formulations, Bif@PDA-PTX-NPs exhibited a stronger anti-tumor effect by improving the efficacy of PTX, and significantly prolonged the survival of tumor-bearing mice. The Bif@PDA-PTX-NPs biohybrid is a promising nanoplatform for targeted therapy of solid tumors.

Supporting Information

Supplementary Figures to this article can be found online.

Data Sharing Statement

All data generated or analyzed during this study are included in this published article and its additional files.

Funding

This study is supported by grants from the Science and Technology Department of Sichuan Province (2020YJ0385, 2022YFS0623-C2), the Key Project of Southwest Medical University (No. 2021ZKZD014), the Youth Fund Projects of Southwest Medical University (No. 2020ZRQNA028), the Science and Technology Project of Luzhou (2022-JYJ-139, 2017LZXNYD-Z04).

Disclosure

The authors declare no competing financial interest in this work.

References

1. Wilson WR, Hay MP. Targeting hypoxia in cancer therapy. *Nat Rev Cancer*. 2011;11(6):393–410. doi:10.1038/nrc3064
2. Manoochehri Khoshinani H, Afshar S, Najafi R. Hypoxia: a double-edged sword in cancer therapy. *Cancer Invest*. 2016;34(10):536–545. doi:10.1080/07357907.2016.1245317
3. Fu J, Wu Q, Dang Y, et al. Synergistic therapy using doxorubicin-loading and nitric oxide-generating hollow Prussian blue nanoparticles with photoacoustic imaging potential against breast cancer. *Int J Nanomedicine*. 2021;16:6003–6016. doi:10.2147/IJN.S327598
4. Muhamad N, Plengsuriyakarn T, Na-Bangchang K. Application of active targeting nanoparticle delivery system for chemotherapeutic drugs and traditional/herbal medicines in cancer therapy: a systematic review. *Int J Nanomedicine*. 2018;13:3921–3935. doi:10.2147/IJN.S165210
5. Zheng P, Fan M, Liu H, et al. Self-Propelled and Near-infrared-phototaxic photosynthetic bacteria as photothermal agents for hypoxia-targeted cancer therapy. *ACS Nano*. 2021;15(1):1100–1110. doi:10.1021/acsnano.0c08068
6. Chen F, Zang Z, Chen Z, et al. Nanophotosensitizer-engineered Salmonella bacteria with hypoxia targeting and photothermal-assisted mutual bioaccumulation for solid tumor therapy. *Biomaterials*. 2019;214:119226. doi:10.1016/j.biomaterials.2019.119226
7. He W, Li X, Morsch M, et al. Brain-targeted codelivery of Bcl-2/Bcl-xl and Mcl-1 inhibitors by biomimetic nanoparticles for orthotopic glioblastoma therapy. *ACS Nano*. 2022;16(4):6293–6308. doi:10.1021/acsnano.2c00320
8. Li Y, Ma X, Yue Y, et al. Rapid surface display of mRNA antigens by bacteria-derived outer membrane vesicles for a personalized tumor vaccine. *Adv Mater*. 2022;34(20):e2109984. doi:10.1002/adma.202109984
9. Chen H, Li Y, Wang Y, et al. An engineered bacteria-hybrid microrobot with the magnetothermal bioswitch for remotely collective perception and imaging-guided cancer treatment. *ACS Nano*. 2022;16(4):6118–6133. doi:10.1021/acsnano.1c11601
10. Yang S, Gao H. Nanoparticles for modulating tumor microenvironment to improve drug delivery and tumor therapy. *Pharmacol Res*. 2017;126:97–108. doi:10.1016/j.phrs.2017.05.004
11. Sang W, Zhang Z, Dai Y, et al. Recent advances in nanomaterial-based synergistic combination cancer immunotherapy. *Chem Soc Rev*. 2019;48(14):3771–3810. doi:10.1039/c8cs00896e

12. Xiong W, Peng L, Chen H, et al. Surface modification of MPEG-b-PCL-based nanoparticles via oxidative self-polymerization of dopamine for malignant melanoma therapy. *Int J Nanomedicine*. 2015;10:2985–2996. doi:10.2147/IJN.S79605
13. Hao Y, Chen Y, He X, et al. Near-infrared responsive 5-fluorouracil and indocyanine green loaded MPEG-PCL nanoparticle integrated with dissolvable microneedle for skin cancer therapy. *Bioact Mater*. 2020;5(3):542–552. doi:10.1016/j.bioactmat.2020.04.002
14. Hu Y, He Y, Ji J, et al. Tumor targeted curcumin delivery by folate-modified MPEG-PCL self-assembly micelles for colorectal cancer therapy. *Int J Nanomedicine*. 2020;15:1239–1252. doi:10.2147/IJN.S232777
15. Danhier F. To exploit the tumor microenvironment: since the EPR effect fails in the clinic, what is the future of nanomedicine? *J Control Release*. 2016;244(Pt A):108–121. doi:10.1016/j.jconrel.2016.11.015
16. Srivastava I, Xue R, Jones J, et al. Biomimetic surface-enhanced Raman scattering nanoparticles with improved dispersibility, signal brightness, and tumor targeting functions. *ACS Nano*. 2022;16(5):8051–8063. doi:10.1021/acsnano.2c01062
17. Barua S, Mitragotri S. Challenges associated with penetration of nanoparticles across cell and tissue barriers: a review of current status and future prospects. *Nano Today*. 2014;9(2):223–243. doi:10.1016/j.nantod.2014.04.008
18. Overchuk M, Zheng G. Overcoming obstacles in the tumor microenvironment: recent advancements in nanoparticle delivery for cancer theranostics. *Biomaterials*. 2018;156:217–237. doi:10.1016/j.biomaterials.2017.10.024
19. Charbonneau MR, Isabella VM, Li N, et al. Developing a new class of engineered live bacterial therapeutics to treat human diseases. *Nat Commun*. 2020;11(1):1738. doi:10.1038/s41467-020-15508-1
20. Zheng DW, Chen Y, Li ZH, et al. Optically-controlled bacterial metabolite for cancer therapy. *Nat Commun*. 2018;9(1):1680. doi:10.1038/s41467-018-03233-9
21. Yi X, Zhou H, Chao Y, et al. Bacteria-triggered tumor-specific thrombosis to enable potent photothermal immunotherapy of cancer. *Sci Adv*. 2020;6(33):eaba3546. doi:10.1126/sciadv.aba3546
22. Wang SB, Liu XH, Li B, et al. Bacteria-assisted selective photothermal therapy for precise tumor inhibition. *Adv Funct Mater*. 2019;29(35):1904093. doi:10.1002/adfm.201904093
23. Deng X, Yang W, Shao Z, et al. Genetically modified bacteria for targeted phototherapy of tumor. *Biomaterials*. 2021;272:120809. doi:10.1016/j.biomaterials.2021.120809
24. Liu Y, Lu Y, Ning B, et al. Intravenous delivery of living listeria monocytogenes elicits gasdermin-dependent tumor pyroptosis and motivates anti-tumor immune response. *ACS Nano*. 2022;16(3):4102–4115. doi:10.1021/acsnano.1c09818
25. Wang L, Vuletic I, Deng D, et al. Bifidobacterium breve as a delivery vector of IL-24 gene therapy for head and neck squamous cell carcinoma in vivo. *Gene Ther*. 2017;24(11):699–705. doi:10.1038/gt.2017.74
26. Jiang BL, Gao X, Xiong J, et al. Experimental study on synergistic effect of HIFU treatment of tumors using Bifidobacterium bound with cationic phase-change nanoparticles. *Eur Rev Med Pharmacol Sci*. 2020;24(10):5714–5725. doi:10.26355/eurrev_202005_21363
27. Xiao S, Shi H, Zhang Y, et al. Bacteria-driven hypoxia targeting delivery of chemotherapeutic drug proving outcome of breast cancer. *J Nanobiotechnol*. 2022;20(1):178. doi:10.1186/s12951-022-01373-1
28. Li Y, Leng Q, Zhang Y, et al. Anaerobic bacteria mediated 'smart missile' targeting tumor hypoxic area enhances the therapeutic outcome of lung cancer. *Chem Eng J*. 2022;438:135566. doi:10.1016/j.cej.2022.135566
29. Lee H, Dellatore SM, Miller WM, et al. Mussel-inspired surface chemistry for multifunctional coatings. *Science*. 2007;318(5849):426–430. doi:10.1126/science.1147241
30. Dai G, Choi CKK, Choi CHJ, et al. Glutathione-degradable polydopamine nanoparticles as a versatile platform for fabrication of advanced photosensitisers for anticancer therapy. *Biomater Sci*. 2021;10(1):189–201. doi:10.1039/D1BM01482J
31. Zhang J, Sun X, Zhao X, et al. Watson-crick base pairing-inspired laser/GSH activatable miRNA-coordination polymer nanoplexes for combined cancer chemo-immuno-photothermal therapy. *ACS Appl Mater Interface*. 2022;14(18):20762–20777. doi:10.1021/acsami.2c03523
32. Wang Q, Li X, Mao J, et al. Biomimic binding affinity gradients triggered GSH-response of core-shell nanoparticles for cascade chemo/chemodynamic therapy. *Adv Healthc Mater*. 2022;11(2):e2101634. doi:10.1002/adhm.202101634
33. Zhou J, Schmid T, Schnitzer S, et al. Tumor hypoxia and cancer progression. *Cancer Lett*. 2006;237(1):10–21. doi:10.1016/j.canlet.2005.05.028
34. Dhani N, Fyles A, Hedley D, et al. The clinical significance of hypoxia in human cancers. *Semin Nucl Med*. 2015;45(2):110–121. doi:10.1053/j.semnuclmed.2014.11.002
35. Zeng Y, Ma J, Zhan Y, et al. Hypoxia-activated prodrugs and redox-responsive nanocarriers. *Int J Nanomedicine*. 2018;13:6551–6574. doi:10.2147/IJN.S173431
36. Wang Y, Xie Y, Li J, et al. Tumor-penetrating nanoparticles for enhanced anticancer activity of combined photodynamic and hypoxia-activated therapy. *ACS Nano*. 2017;11(2):2227–2238. doi:10.1021/acsnano.6b08731
37. Taniguchi S, Fujimori M, Sasaki T, et al. Targeting solid tumors with non-pathogenic obligate anaerobic bacteria. *Cancer Sci*. 2010;101(9):1925–1932. doi:10.1111/j.1349-7006.2010.01628.x
38. Zhao M, Yang M, Li XM, et al. Tumor-targeting bacterial therapy with amino acid auxotrophs of GFP-expressing *Salmonella typhimurium*. *Proc Natl Acad Sci USA*. 2005;102(3):755–760. doi:10.1073/pnas.0408422102
39. Pawelek JM, Low KB, Bermudes D. Tumor-targeted Salmonella as a novel anticancer vector. *Cancer Res*. 1997;57(20):4537–4544.
40. Tang Y, Chen C, Jiang B, et al. Bifidobacterium bifidum-mediated specific delivery of nanoparticles for Tumor Therapy. *Int J Nanomedicine*. 2021;16:4643–4659. doi:10.2147/IJN.S315650
41. Dang LH, Bettegowda C, Huso DL, et al. Combination bacteriolytic therapy for the treatment of experimental tumors. *Proc Natl Acad Sci USA*. 2001;98(26):15155–15160. doi:10.1073/pnas.251543698
42. Jain RK, Forbes NS. Can engineered bacteria help control cancer? *Proc Natl Acad Sci USA*. 2001;98(26):14748–14750. doi:10.1073/pnas.261606598
43. Fan JX, Peng MY, Wang H, et al. Engineered bacterial bioreactor for tumor therapy via Fenton-like reaction with localized H_2O_2 generation. *Adv Mater*. 2019;31(16):e1808278. doi:10.1002/adma.201808278
44. Zhang W, Liu J, Li X, et al. Precise chemodynamic therapy of cancer by trifunctional bacterium-based nanozymes. *ACS Nano*. 2021;15(12):19321–19333. doi:10.1021/acsnano.1c05605
45. Kuo WS, Wu CM, Yang ZS, et al. Biocompatible bacteria@Au composites for application in the photothermal destruction of cancer cells. *Chem Commun (Camb)*. 2008;37(7):4430–4432. doi:10.1039/b808871c

46. Farokhi M, Mottaghitalab F, Saeb MR, et al. Functionalized theranostic nanocarriers with bio-inspired polydopamine for tumor imaging and chemo-photothermal therapy. *J Control Release*. 2019;309:203–219. doi:10.1016/j.jconrel.2019.07.036
47. Zhang Z, Zhang J, Tian J, et al. A polydopamine nanomedicine used in photothermal therapy for liver cancer knocks down the anti-cancer target NEDD8-E3 ligase ROC1 (RBX1). *J Nanobiotechnol*. 2021;19(1):323. doi:10.1186/s12951-021-01063-4
48. Hao YN, Zheng AQ, Guo TT, et al. Glutathione triggered degradation of polydopamine to facilitate controlled drug release for synergic combinational cancer treatment. *J Mater Chem B*. 2019;7(43):6742–6750. doi:10.1039/C9TB01400D
49. Kennedy L, Sandhu JK, Harper ME, et al. Role of glutathione in cancer: from mechanisms to therapies. *Biomolecules*. 2020;10(10):1429. doi:10.3390/biom10101429
50. Chen W, Wang Y, Qin M, et al. Bacteria-driven hypoxia targeting for combined biotherapy and photothermal therapy. *ACS Nano*. 2018;12(6):5995–6005. doi:10.1021/acsnano.8b02235
51. Lu J, Cai L, Dai Y, et al. Polydopamine-based nanoparticles for photothermal therapy/chemotherapy and their synergistic therapy with autophagy inhibitor to promote antitumor treatment. *Chem Rec*. 2021;21(4):781–796. doi:10.1002/tcr.202000170
52. Yan S, Huang Q, Chen J, et al. Tumor-targeting photodynamic therapy based on folate-modified polydopamine nanoparticles. *Int J Nanomedicine*. 2019;14:6799–6812. doi:10.2147/IJN.S216194